CHAPTER 1

NEGATIVE FEEDBACK BY CALCIUM: THE ROAD FROM CHAY-KEIZER

Richard Bertram
Department of Mathematics and Institute of Molecular Biophysics
Florida State University
Tallahassee, FL 32306, U. S. A.
E-mail: bertram@sb.fsu.edu

Arthur Sherman
Laboratory of Biological Modeling, NIDDK
National Institutes of Health
Bethesda, MD 20892, U. S. A.
E-mail: asherman@nih.gov

Add abstract here.

1. Introduction

One of the earliest bursting models was not for a neural system, but for the insulin-secreting pancreatic β-cell. This cell type is of great interest because defects in insulin secretion are important for the pathogenesis of Type 2 Diabetes Mellitus (T2DM). In fact, in recent years data has accumulated implicating electrical properties of β-cells, specifically channel polymorphisms, in T2DM (Ashcroft and Rorsman 2004).

Here, however, our focus will be on two other aspects of the Chay-Keizer (CK) model (Chay and Keizer, 1983). One is the underlying bifurcation structure of the model, which is square-wave (Rinzel, 1987) or fold-homoclinic (Izhikevich, 2000) or Type I bursting (Bertram *et al.*, 1995). This easy-to-understand pattern has provided a template for a number of other important models, some of which are reviewed in this book, including the Hindmarsh-Rose model for thalamic neurons (Hindmarsh and Rose, 1984), the Butera-Rinzel-Smith model for respiratory pacemaker neurons

in the pre-Bötzinger complex (Butera *et al.*, 1999), and the Tabak-Rinzel-O'Donovan model for episodic network activity in embryonic spinal cord (Tabak *et al.*, 2001).

A second aspect of general interest is the paradigm of slow negative feedback by cytosolic Ca^{2+}, which in CK targets a Ca^{2+}-activated K^+ channel. This was a natural choice following the success of the early Plant model for the R-15 neuron (Plant, 1978). However, this seductive hypothesis has traveled a hard road, falling into disfavor before the age of 10 and making a comeback before the age of 20. The Ca^{2+}-feedback hypothesis has emerged from these trials altered, but still recognizable, and strengthened by insights into new areas of cellular Ca^{2+} handling, including sequestration and release by the endoplasmic reticulum (ER) and exotic effects on metabolism, including mitochondrial respiration and glycolytic oscillations.

In addition, we have found that the simplest square-wave burster models, with a single slow variable, are not adequate to account for the complexity of β-cell activity patterns. Adding a second or third slow variable, while mathematically redundant, greatly enhances the robustness and dynamic range and leads to qualitative changes in some properties, such as phase resetting.

In this chapter we will trace out a pedagogically streamlined history of the twin ideas of square-wave bursting and calcium feedback, focusing in detail on the properties of the ER.

2. Before the Beginning

The square-wave bursting typcial of β-cells is dynamically similar to a relaxation oscillation. The prototypical relaxation oscillator was developed by van der Pol and van der Mark as a description of an oscillatory cardiac pacemaker (van der Pol and van der Mark, 1928). Later, FitzHugh and Nagumo developed simple neural models, recognizing that an action potential or electrical impulse could be described as a relaxation oscillation (FitzHugh, 1961; Nagumo *et al.*, 1964). The key features of what was to be called the FitzHugh-Nagumo model are (1) a cubic voltage nullcline, and (2) a separation of time scales of the two variables, so that one changes much more rapidly than the other. The Morris-Lecar model for a barnacle muscle fiber, developed two decades later, also possesses these features, although the voltage nullcline is only approximately cubic in this case (Morris and Lecar, 1981). Because Morris-Lecar includes expressions for ionic currents, it is more suitable for describing biophysical phenomena, such as the effects

of channel blockers.

We use a modification of the Morris-Lecar model to describe impulses in the β-cell:

$$C_m \frac{dV}{dt} = -[I_{Ca} + I_K + I_{K(Ca)} + I_{K(ATP)}] \tag{1}$$

$$\frac{dn}{dt} = \lambda(n_\infty(V) - n)/\tau_n \ , \tag{2}$$

where C_m is the membrane capacitance of the cell, V is membrane potential or voltage, I_{Ca} is an inward Ca^{2+} current, I_K is an outward K^+ current of the delayed rectifier type, $I_{K(Ca)}$ is a Ca^{2+}-activated K^+ current and $I_{K(ATP)}$ is an ATP-sensitive K^+ current (ATP=adenosine triphosphate). The latter two currents, $I_{K(Ca)}$ and $I_{K(ATP)}$, were not included in the Morris-Lecar model, but have been added here because they play important roles in β-cells. Additional variables and parameters in the model are n, the activation variable for I_K, its equilibrium function $n_\infty(V)$, and its activation time constant, τ_n. The parameter λ is used as a convenient means to speed up or slow down the time scale of the variable n. Additional equations are:

$$I_{Ca} = g_{Ca} m_\infty(V)(V - V_{Ca}) \tag{3}$$

$$I_K = g_K n(V - V_K) \tag{4}$$

$$I_{K(Ca)} = g_{K(Ca)} \left(\frac{c^3}{c^3 + K_d^3} \right) (V - V_K) \tag{5}$$

$$I_{K(ATP)} = g_{K(ATP)}(V - V_K) \tag{6}$$

$$m_\infty(V) = [1 + \exp((v_m - V)/s_m)]^{-1} \tag{7}$$

$$n_\infty(V) = [1 + \exp((v_n - V)/s_n)]^{-1} \ . \tag{8}$$

With the parameter values listed in Table 1 the system is oscillatory, producing a continuous train of impulses. One of these is shown in Fig. 1A. This impulse is characterized by a rapid upstroke (due to the inward current I_{Ca}) and a rapid downstroke (due to the outward current I_K), with slow changes between impulses. Figure 1B illustrates the impulse trajectory (oriented curve) in the nV-phase plane. The scaling parameter λ is small in this simulation ($\lambda = 0.01$), so the activation variable n changes much more slowly than V. As a result, the trajectory is attracted to the V-nullcline, and moves along either the top or bottom branch of the cubic until the branch switches back. The trajectory moves slowly to the left (since $dn/dt < 0$) along the bottom branch between impulses. When the branch ends the trajectory moves rapidly to the top branch and travels

rightward (since $dn/dt > 0$) until this branch ends, after which the trajectory moves rapidly to the lower branch. Motion along the upper branch and the rapid transitions between branches constitute the impulse. The full orbit is a classic relaxation oscillation. It is important that the nullclines intersect only along the middle branch of the V-nullcline. Otherwise, the intersection point, a steady state of the system, would be stable and periodic motion would not occur.

Table 1: Parameter Values for the Morris-Lecar Model

Parameter	Value	Parameter	Value
g_{Ca}	1000 pS	g_K	2700 pS
$g_{K(Ca)}$	400 pS	$g_{K(ATP)}$	180 pS
V_{Ca}	25 mV	V_K	-75 mV
C_m	5300 fF	λ	1
τ_n	20 msec	K_D	0.4 μM
v_n	-16 mV	s_n	5 mV
v_m	-20 mV	s_m	12 mV

In most β-cell models the time scale separation is not as extreme as in this example. Thus, rather than $\lambda = 0.01$ a value closer to $\lambda = 1$ is used. With the n dynamics now 100 times faster, the trajectory no longer rides along the branches of the V-nullcline, but instead travels along an elliptical path between the upper and lower branches of the nullcline. The resulting impulse is of lower amplitude, with peak value less than -10 mV (Fig. 2A). For more detailed phase-plane analysis see Sherman (1997) and corresponding exercises at http://mrb.niddk.nih.gov/sherman, where the equations used here may also be found. Smaller impulses like these are characteristic of impulses recorded in β-cells (Zhang *et al.*, 2003). For the remainder of this chapter we use $\lambda = 1$.

Calcium-activated K^+currents, $I_{K(Ca)}$, are found in many neurons (Hille, 2001). In β-cells, Ca^{2+}-activated and voltage-independent K(Ca) channels were originally thought to be responsible for packaging impulses into bursts (Atwater *et al.*, 1980), which led to the Chay-Keizer model described in the next section. For now we treat the cytosolic Ca^{2+} concentration, c, as a parameter. Increasing this parameter increases the outward K(Ca) current (Eq. 5), which has a hyperpolarizing effect on the cell. In terms of the phase plane, increasing c translates the V-nullcline leftward (Fig. 2B). This may result in an intersection of the two nullclines on the

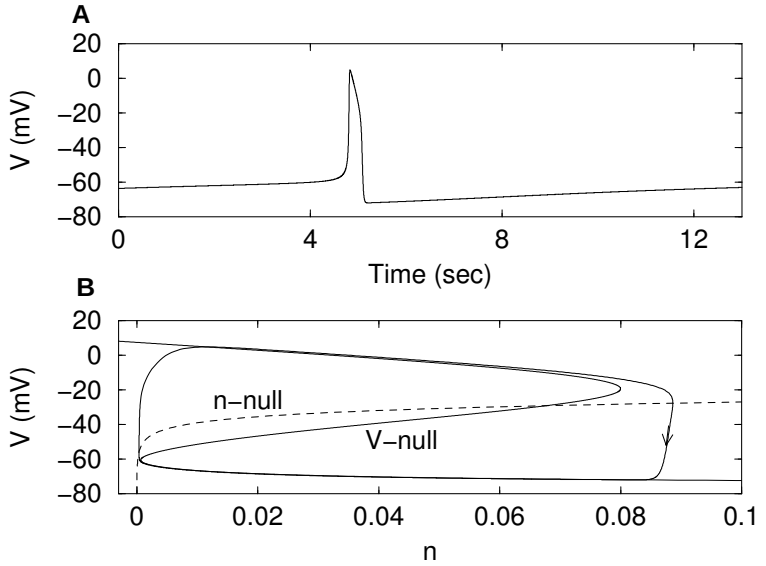

Fig. 1. (**A**) A single impulse from a train of impulses generated by the Morris-Lecar-like model. (**B**) Phase plane view of an impulse. The trajectory (oriented curve) moves along the top and bottom branches of the V-nullcline, and is a typical relaxation oscillation. The time scale parameter is small, $\lambda = 0.01$, accentuating the separation in time scales of the V and n variables. Cytosolic calcium, c, is fixed at 0.1 μM.

lower branch of the V-nullcline, creating a hyperpolarized stable steady state (indicated by a circle). When this occurs the system moves from a state of continuous spiking to a resting state at a low voltage (Fig. 2A). Thus, the dynamics of the system depend critically on the cytosolic Ca^{2+} concentration.

The scenarios described in Fig. 2 reflect two extreme cases, where the system has either a globally attracting periodic solution or a globally attracting steady state. An important intermediate case occurs for $1 < c < 2$. Here, a stable periodic solution coexists with a stable steady state (Fig. 3). There are three steady state solutions. The solution with the highest voltage (open circle) is an unstable spiral, which is surrounded by a stable limit cycle. The middle steady state solution (open triangle) is a saddle point, whose stable manifold (dot-dashed curve) forms the separatrix between the basins of attraction of the stable limit cycle and the stable steady state (filled circle). In this *bistable system* the ultimate fate of a trjectory is de-

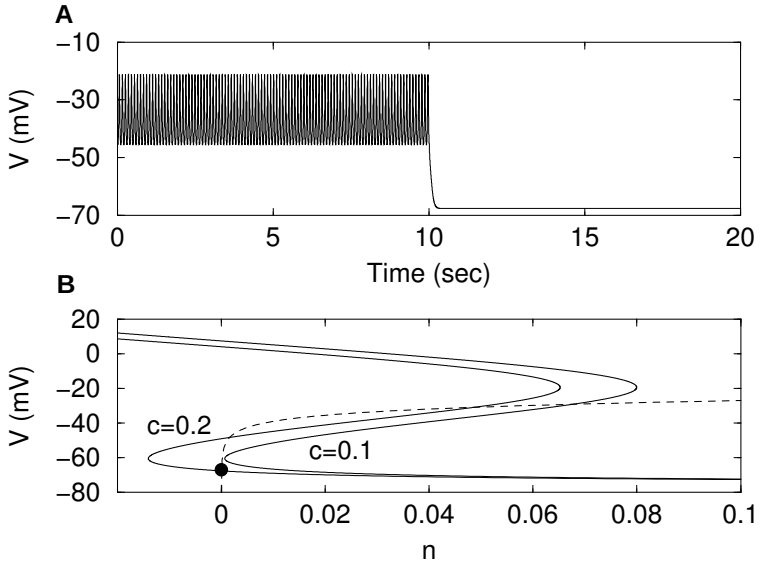

Fig. 2. (**A**) A train of β-cell-like impulses is terminated when the cytosolic Ca^{2+} concentration is increased from $c = 0.1$ to $c = 0.2$. (**B**) Increasing c from 0.1 to 0.2 shifts the V-nullcline leftward. The filled circle represents a stable steady-state solution.

termined by its starting location. If the trajectory starts between the two branches of the stable manifold, then it is attracted to the limit cycle. If it starts below this region then the trajectory is attracted to the stable steady state. We shall see below that bistability between a steady state and a periodic solution is the key ingredient for square-wave bursting.

3. The Beginning

All current models for β-cellelectrical activity are descendants of the Chay-Keizer model (1983). Even though this model did not contain all of the features subsequently shown to be important in β-cell electrical activity, it successfully identified the key elements of square-wave bursting and provided a scaffold onto which additional elements could be added. The appealing simplicity accounts for its impact on bursting models in general. Chay-Keizer was based on the earlier hypothesis of Atwater and Rojas that bursting is due to the slow rise and fall of the cytosolic Ca^{2+} concentration, acting on K(Ca) channels (Atwater *et al.*, 1980).

Historically, however, Chay-Keizer was preceded by a less well-known

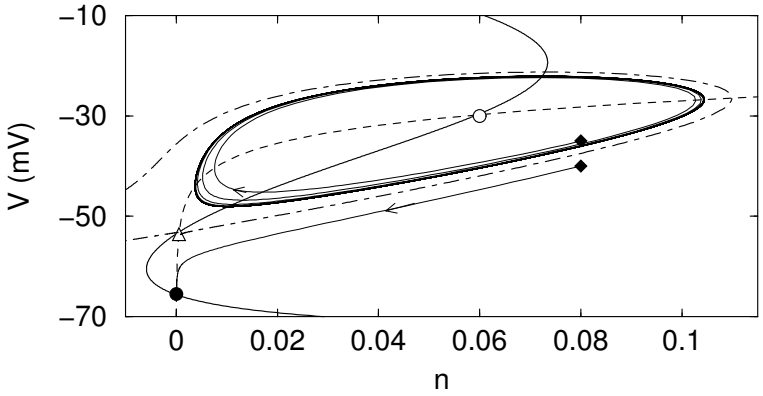

Fig. 3. For intermediate values of the parameter c (here $c = 0.15$) the system is bistable. A stable limit cycle coexists with a stable hyperpolarized steady state (filled circle). Trajectories starting within the two branches of the saddle point's stable manifold (dot-dashed curve) are attracted to the limit cycle. Those starting below this region are attracted to the stable steady state.

model developed by Matthews and O'Connor (1979). It anticipated many features of Chay-Keizer, such as a central role for K(Ca) channels, as well as features not introduced until much later, such as metabolic oscillations. However, the Matthews-O'Connor model was much more complex than Chay-Keizer because special currents were assigned roles in producing the plateau and pacemaker functions, roles that arose organically from a much simpler set of currents in Chay-Keizer. This perhaps accounts for why it left no apparent progeny and serves as a lesson on the virtue of knowing what data to ignore when beginning to develop a model.

Chay and Keizer used modified squid axon Hodgkin-Huxley equations (Hodgkin and Huxley, 1952) to describe action potentials. We use the simpler Morris-Lecar model, supplemented by a differential equation for the cytosolic Ca^{2+} concentration:

$$\frac{dc}{dt} = f_{cyt} J_{mem} \quad , \tag{9}$$

where c is the cytosolic Ca^{2+} concentration, f_{cyt} is the fraction of cytosolic Ca^{2+} that is not bound to buffers, and J_{mem} is the Ca^{2+} flux across the plasma membrane. The Ca^{2+} influx is through Ca^{2+} channels and the efflux is through Ca^{2+} pumps (Ca^{2+} ATPases):

$$J_{mem} = -(\alpha I_{Ca} + k_{pmca} c) \quad , \tag{10}$$

where α converts current to flux, and k_{pmca} is the pump rate.

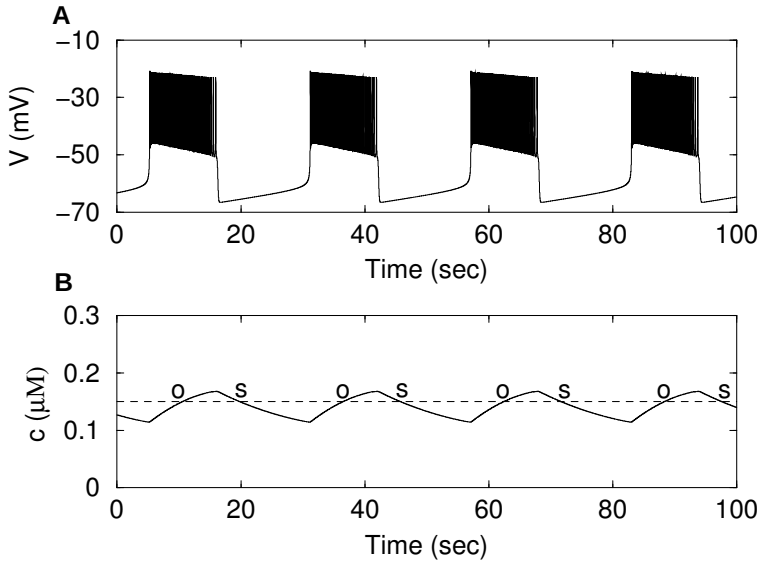

Fig. 4. (**A**) Bursting produced by the Chay-Keizer model. (**B**) Bursting is driven by slow activity-dependent oscillations in the cytosolic Ca^{2+} concentration. The Ca^{2+} concentration rises during the active phase and falls during the silent phase of bursting. The horizontal dashed line is used to illustrate that the fast subsystem is bistable: for the same value of c the fast subsystem may be oscillatory ("O") or stationary ("S"). Fraction of free Ca^{2+} is $f_{cyt} = 0.00025$.

This three-variable model is able to reproduce the square-wave bursting that characterizes β-cells (Fig. 4A). During the oscillatory or active phase, Ca^{2+} channels are mostly open, so that Ca^{2+} accumulates in the cell. Thus, c rises during the active phase ("O" in Fig. 4B). This rise is slow, since the effective time scale for c is large. (The time scale can be easily adjusted using the parameter f_{cyt}, which is currently set to a very small value, $f_{cyt} = 0.00025$.) The rise in c activates K(Ca) current, translating the V-nullcline leftward (Fig. 2). Eventually c rises to a large enough value that the V- and n-nullclines intersect, terminating the active phase of spiking. Now that the system has entered the silent phase and V is in a low rest state the Ca^{2+} channels close. This results in a slow decline in c ("S" in Fig. 4B). As a result, hyperpolarizing K(Ca) current is shut off and the V-nullcline is translated rightward. Eventually, the stable intersection of the V- and

n-nullclines is lost and the system re-enters the oscillatory active phase. Note that the burst period is on the order of tens of seconds (here about 22 sec). This is typical of most *in vitro* electrical recordings from β-cells within intact islets, but is very slow compared with bursting produced by most neurons.

A standard way to analyze bursting oscillations is to separate the variables into slow and fast subsystems, and then to treat the slow variable as a parameter of the fast subsystem. This "fast/slow analysis" was pioneered by John Rinzel, and used to analyze several types of bursting oscillations, including the square-wave bursting characteristic of β-cells (Rinzel and Lee, 1985; Rinzel, 1987). In our case, the fast subsystem consists of Eqs. 1–2, with fast variables V and n. The calcium concentration c is the single slow variable. For large values of c, now treated as a parameter of the fast subsystem, the V nullcline is shifted far to the left (see Fig. 2) and the model cell is silent at a hyperpolarized voltage. As c is reduced the V nullcline is translated rightward, so the intersection with the n-nullcline occurs at higher voltages. For sufficiently small values of c the lower knee of the V-nullcline is to the right of the n-nullcline. That is, a saddle-node bifurcation (SN) has occurred. This is illustrated in the bifurcation diagram of Fig. 5. The lower branch of this diagram corresponds to the lower, stable, steady state of the fast subsystem. The middle, unstable, branch corresponds to steady states on the middle branch of the V-nullcline, and is a branch of saddle points. This saddle point branch begins at the SN bifurcation with the stable steady state branch, and ends at a second SN bifurcation with a branch of unstable equilibria. The SN bifurcations are marked by triangles in Fig. 5.

The branch of upper unstable equilibria continues for lower values of c, and eventually goes through a supercritical Hopf bifurcation (circle). Beyond this the branch is stable. A branch of stable periodic solutions emerges from the Hopf bifurcation. Each of these periodic solutions represents a continuous train of action potentials (as in the left portion of Fig. 2). The periodic branch terminates at a homoclinic bifurcation, where the limit cycle connects with a saddle point, forming an infinite-period homoclinic orbit. The bistability illustrated in Fig. 3 occurs for all values of c between the left SN (triangle) and the homoclinic bifurcation (square).

The z-shaped fast-subsystem bifurcation diagram, called the "slow manifold" or "z-curve", is defined as the curve on which V and n are at steady state and can be constructed numerically using XPPAUT by treating c as a parameter. The z-curve can also be calculated analytically by defining the

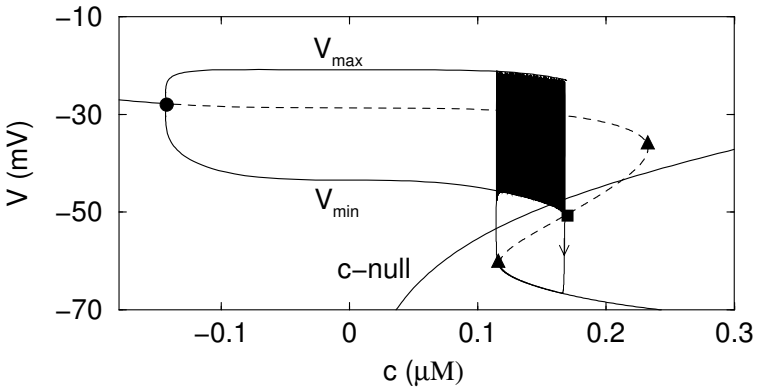

Fig. 5. Fast/slow analysis of bursting. The burst trajectory and c-nullcline are superimposed on a bifurcation diagram (z-curve) of the fast subsystem. On the z-curve, solid curves represent stable solutions and dashed curves represent unstable solutions. There are two saddle-node bifurcations (triangles), a supercritical Hopf bifurcation (circle), and a homoclinic bifurcation (square). The periodic branch is represented using the minimum (V_{min}) and maximum (V_{max}) voltage of the oscillations.

fraction of activated K(Ca) channels,

$$\omega = \frac{c^3}{c^3 + K_d^3}, \tag{11}$$

solving Eq. 1 for ω,

$$\omega = -\frac{g_{Ca} m_\infty(V)(V - V_{Ca}) + g_K n(V - V_K)}{g_{K(Ca)}(V - V_K)} + \frac{g_{K(ATP)}}{g_{K(Ca)}}, \tag{12}$$

and solving Eq. 11 for c.

We now add in the slow dynamics of c, and view Fig. 5 as a c-V phase plane. The c-nullcline, obtained from Eq. 9, is superimposed. Below the nullcline $dc/dt < 0$, while above the nullcline $dc/dt > 0$. Finally, we superimpose the burst trajectory. This moves along the z-curve since the fast subsystem dynamics are much faster than the slow subsystem dynamics. This relaxation-like oscillation is similar to the relaxation oscillation shown in Fig. 1. The burst trajectory rides along the bottom branch of the z-curve during the silent phase, traveling to the left since it is below the c-nullcline. When the trajectory reaches the SN bifurcation it moves to the periodic branch, since the limit cycle is now the only remaining attractor. At this point the trajectory travels rightward since it is above the c-nullcline. The

active pase of bursting ends when the trajectory reaches the homoclinic bifurcation. This completes one cycle of bursting.

The bistability of the fast subsystem is a crucial feature of square-wave bursting. Without bistability there would be no bursting. Also, bursting does not occur if the c-nullcline intersects the lower branch of the z-curve, since in this case the intersection is a stable equilibrium of the full system of equations. Likewise, if the nullcline crosses deep into the periodic branch the system will spike continuously. Thus, for bursting to occur, the c-nullcline must cross the z-curve either between the lower SN and the homoclinic bifurcation, or slightly above the homoclinic bifurcation. If the slow variable were infinitely slow then bursting would occur only if the crossing occurs between the saddle node and the homoclinic bifurcation (Terman, 1992).

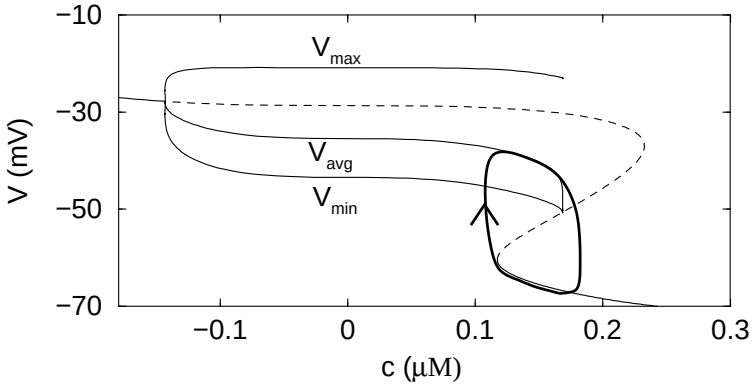

Fig. 6. The z-curve is similar in shape to the cubic V-nullcline of the Morris-Lecar relaxation oscillator when the periodic branch is represented by the average voltage curve.

The similarity between the fast/slow analysis of bursting and the dynamics of a relaxation oscillation is emphasized in Fig. 6. Here the periodic branch is represented not only by the maximum and minimum voltage curves, but also by a curve showing the average voltage (V_{avg}). The average voltage of the burst trajectory then travels along the average V branch during the active phase, and the lower branch of the z-curve during the silent phase (Fig. 6, heavy curve). (We note that the equivalent V curve, V_{eqv}, is more representative of the periodic branch than the average V curve (Bertram *et al.*, 1995). However, V_{avg} is much easier to compute, and

is in many cases, including this one, a sufficiently good approximation of V_{eqv}.) The union of the z-curve with the V_{avg} curve is then analogous to the V-nullcline in the relaxation oscillator of Fig. 1.

In addition to exhibiting bursting, Chay-Keizer was able to reproduce the effects on membrane potential of increasing the glucose concentration. This is physiologically important because β-cells adjust their output (insulin secretion) according to the glucose level in the blood. The insulin secretion rate is roughly proportional to the *plateau fraction*, the ratio of the active phase duration to the total burst period. At low glucose levels the cell is silent, so the plateau fraction is 0 and the rate of insulin secretion is low. With glucose concentrations just beyond about 5 mM the β-cells burst, but the plateau fraction is relattively low, < 0.5. As the glucose concentration is increased, the plateau fraction increases, raising the mean rate of insulin secretion. At very high glucose concentrations, ≈ 20 mM, the cell spikes continuously and the plateau fraction reaches a value of 1 (Beigelman *et al.*, 1977).

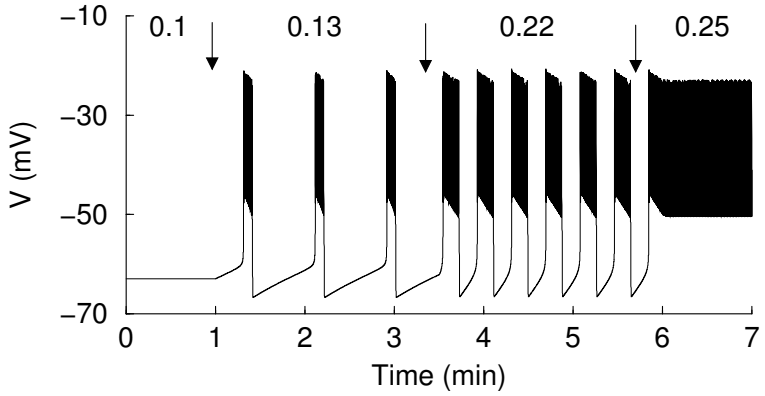

Fig. 7. Simulation of a gradual increase in the glucose concentration. The parameter k_{pmca} is increased from 0.1 to 0.13, then 0.22, and finally 0.25 (at arrows). The response of the model is similar to what has been observed in islets (Beigelman *et al.*, 1977). Fraction of free Ca^{2+} is $f_{cyt} = 0.00025$.

Chay and Keizer simulated the effect of glucose by increasing the Ca^{2+} pump rate k_{pmca}. This is biophysically reasonable, since Ca^{2+} pumps are powered by ATP, and the ATP level in the β-cell increases when the glucose level is increased. Figure 7 shows that the mechanism used by Chay and

Keizer to simulate an increase in the glucose level is able to reproduce the glucose effect on the β-cell's electrical activity. In this figure, k_{pmca} is increased from 0.1, to 0.13, 0.22, and 0.25. With each step increase in k_{pmca} the duration of the silent phase decreases while the duration of the active phase increases, until the cell finally enters a continuous spiking state. In terms of the fast/slow analysis, the c-nullcline is translated upward when k_{pmca} is increased. This increases the distance between the nullcline and the bottom branch of the z-curve, so the trajectory traverses this branch more quickly and the silent phase duration is reduced. At the same time, the distance between the nullcline and the periodic branch (or V_{avg} curve) is decreased, so that the trajectory moves more slowly along this branch, increasing the duration of the active phase. With k_{pmca} small the nullcline intersects the bottom branch of the z-curve and the model cell is at rest. With k_{pmca} large the nullcline intersects deep into the periodic branch and the cell spikes continuously.

It is now believed that a factor more important than Ca^{2+} pumps is the inhibitory effect that glucose has on ATP-sensitive K^+ channels (Ashcroft *et al.*, 1984). When these channels were discovered after the Chay-Keizer model was published, it was easy to demonstrate that reduction of $g_{K(ATP)}$ could also increase plateau fraction (Rinzel *et al.*, 1986). Geometrically, increasing k_{pmca} moves the c nullcline to the left (Eqs. 9, 10), whereas reducing $g_{K(ATP)}$ moves the z-curve to the right (Eq. 12), both of which prolong the active phase at the expense of the silent phase. [We may need to put some more c nullclines in Fig. 5. - AS]

Another feature of islet behavior captured by the Chay-Keizer model is the ability to reset. That is, the model predicts that it should be possible to reset the system from the silent phase to the active phase, and vice versa, by giving a brief voltage perturbation. This is due to the bistability of the fast subsystem (Fig. 8). Furthermore, when the system is reset from the silent phase to the active phase, the active phase should be shorter than usual. This is because the distance that the trajectory must travel along the periodic branch is less than during a typical active phase. The same can be said for resetting from active to silent phase. Thus, the model predicts that resetting is phase-dependent.

Resetting experiments were performed on islets by Cook *et al.* (1980). They found that it was possible to reset an islet from one phase of bursting to the other, consistent with the model. However, this resetting was phase-independent, contrary to the Chay-Keizer model. That is, when the islet was reset from the silent phase to the active phase (or active to silent), the

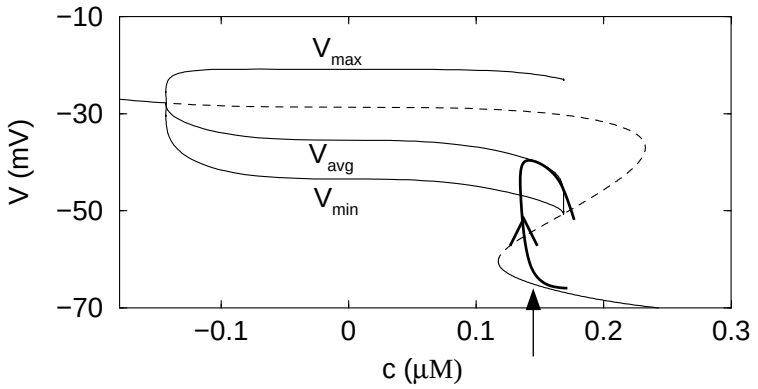

Fig. 8. The Chay-Keizer model predicts that it should be possible to reset from the silent phase to the active phase (at arrow). The active phase is shorter than usual. Resetting should also be possible from the active phase to the silent phase.

active phase duration was similar to that of a typical active phase. A later modeling study suggested one explanation for this behavior (Smolen and Sherman, 1994). Although the Chay-Keizer model failed in this respect, it still established the important principle that bursting oscillations based on bistability are resettable. This is in contrast to bursting oscillations driven by an endogenous oscillatory process, such as the glycolytic oscillations discussed later in this chapter.

4. The Demise of K(Ca)

The most obvious prediction of the Chay-Keizer model is that the cytosolic Ca^{2+} concentration rises slowly during the active phase and declines slowly during the silent phase (Fig. 4B). When Ca^{2+} was first measured some years after publication of the model, it did indeed show clear oscillations (Valdeolmillos *et al.*, 1989). However, these oscillations did not have the sawtooth shape that was predicted by the model. Instead, the concentration often shows two time scales, a rapid rise to a plateau followed by a slowly rising plateau, and a similar pattern in the silent phase (Fig 9A). Even worse, some records showed Ca^{2+} declining before the end of the active phase (Fig. 9B). These measurements seemed to be incompatible with a burst mechanism driven by Ca^{2+} acting on K(Ca) channels.

With cytosolic Ca^{2+} out of favor as a slow variable to drive bursting, a succession of other models with different slow variables was proposed. These

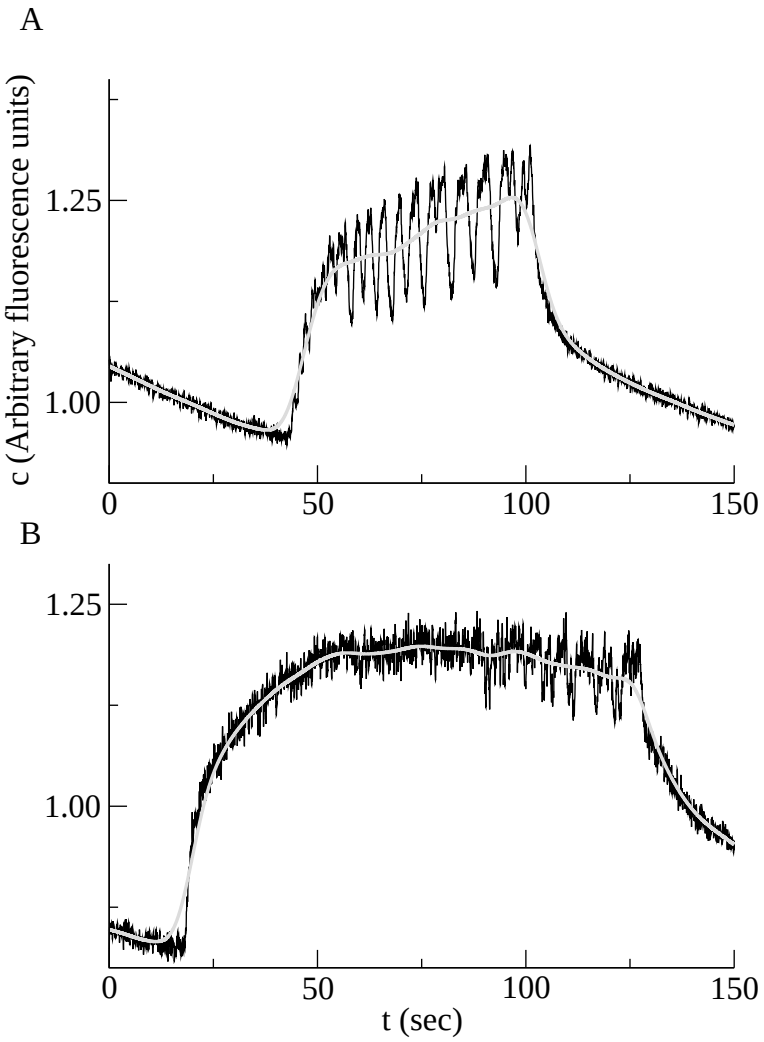

Fig. 9. Cytosolic Ca^{2+} in islets imaged with fura-2. The black curves represent the raw data in arbitrary fluorescence ratio units, and the grey curves are the data smoothed to highlight the trends. Data courtesy of Craig Nunemaker and Les Satin, Virginia Commonwealth University.

included slow inactivation of a voltage-dependent Ca^{2+} current (Chay and Cook, 1988; Keizer and Smolen, 1991); slow changes in the ratio of ATP to ADP, acting on K(ATP) channels (Keizer and Magnus, 1989; Smolen

and Keizer, 1992); and the effects of the endoplasmic reticulum (ER) acting either indirectly on cytosolic Ca^{2+} or directly through Store-Operated-Current (Chay, 1996, 1997). The mathematical template established by the Chay-Keizer model made it relatively easy to devise new models, but in the end none of these survived experimental testing in its pure form.

5. The Return of K(Ca): Help from the Endoplasmic Reticulum

Although not fully appreciated at the time, the most important advance following the Chay-Keizer model was Chay's addition of the ER. This organelle is a storehouse for Ca^{2+}, maintaining a free Ca^{2+} level on the order of hundreds of micromolar (by comparison, the cytosolic free Ca^{2+} concentration never reaches 1 μM.) The ER acts as both a Ca^{2+} source and a Ca^{2+} sink (Bertram and Sherman, 2004b). When the cell is spiking, Ca^{2+} enters the cytosol through Ca^{2+} channels and some of this is transported into the ER through Ca^{2+} pumps in the ER membrane called SERCA pumps (Sarco- and Endoplasmic Reticulum Calcium pumps). Thus, the ER acts as a sink during the active phase of bursting. When the cell is silent, Ca^{2+} channels are closed and there is a net efflux from the cell due to the plasma membrane Ca^{2+} pumps. At the same time, Ca^{2+} enters the cytosol from the ER due to Ca^{2+} leakage across the ER membrane. Thus, the ER acts as a Ca^{2+} source during the silent phase of bursting. The actions of the ER therefore provide a slow component to the cytosolic Ca^{2+} concentration.

With the addition of the ER, the Ca^{2+} subsystem becomes

$$\frac{dc}{dt} = f_{cyt}(J_{mem} - J_{er}) \tag{13}$$

$$\frac{dc_{er}}{dt} = f_{er}\frac{\nu_{cyt}}{\nu_{er}}J_{er} \tag{14}$$

$$= f_{cyt}\sigma_{er}J_{er} \ , \tag{15}$$

where $\sigma_{er} = \frac{\nu_{cyt}/f_{cyt}}{\nu_{er}/f_{er}}$ is the ratio of effective cytosolic to ER volume, J_{mem} is given by Eq. 10, and

$$J_{er} = J_{serca} - J_{leak} \tag{16}$$

where $J_{serca} = k_{serca}c$ is the flux into the ER through SERCA pumps and $J_{leak} = p_{leak}(c_{er} - c)$ is the leak out of the ER into the cytosol. An additional term could be added to J_{er} to account for flux out of the ER through IP_3 receptors/channels, but here we assume that this term is zero

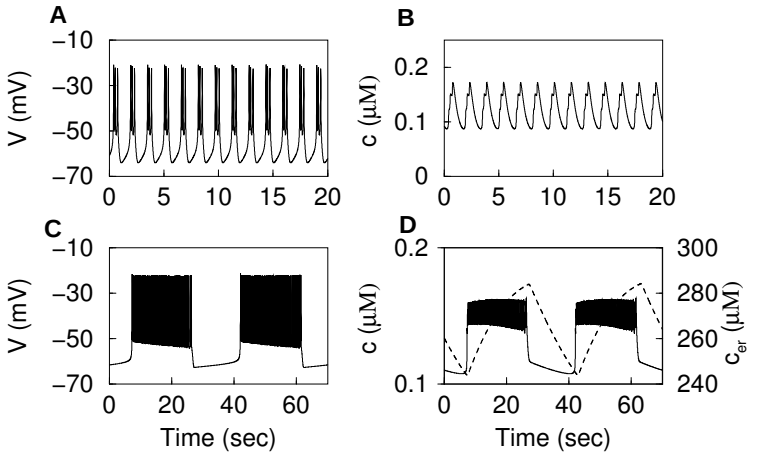

Fig. 10. (**A**) The Chay-Keizer model with the fraction of free cytosolic Ca^{2+} increased by a factor of 40 produces fast bursting ($f_{cyt} = 0.01$, $g_{K(Ca)} = 500$ pS, $g_{K(ATP)} = 185$ pS). (**B**) The cytosolic Ca^{2+} concentration has a sawtooth shape. (**C**) When an ER compartment is added to the model the bursting slows down dramatically. (**D**) Cytosolic Ca^{2+} now has a square shape with a slow decline, similar to experimental measurements. The model predicts that the ER Ca^{2+} concentration (dashed) has a sawtooth shape.

(no muscarinic agonist is present). Details of the model with ER can be found in Bertram and Sherman (2004a).

Table 2: Additional Parameter Values for the Chay-Keizer Model with ER

Parameter	Value	Parameter	Value
f_{cyt}	0.01	k_{pmca}	0.18 msec^{-1}
α	4.5×10^{-6} fA^{-1} μM msec^{-1}	f_{er}	0.01
k_{SERCA}	0.4 msec^{-1}	p_{leak}	0.0002 msec^{-1}
ν_{cyt}	10 μm^3	ν_{er}	0.3 μm^3

Figure 10 illustrates the bursting and Ca^{2+} oscillations produced by the Chay-Keizer model without (panels A and B) and with (panels C and D) an ER. The fraction of Ca^{2+} in the cytosol that is free (f_{cyt}) has been increased from 0.00025 to a more physiological value of 0.01. The effect of this change is to speed up changes in c by a factor of 40. Thus, with this change the Chay-Keizer model bursts with a short period of a few seconds (Fig. 10A). The time course of the cytosolic Ca^{2+} concentration has a sawtooth shape,

reflecting its role in driving the bursting.

The parameter f_{cyt} reflects the amount of Ca^{2+} buffer present in the model cell. A small value of f_{cyt} represents a large concentration of buffer, so that little of the Ca^{2+} that enters the cell remains free. Comparing Fig. 4A with Fig. 10A we see that when the buffer concentration is high, the bursting produced by the Chay-Keizer model is slow. Note that changing f_{cyt} does not change either the z-curve or the c-nullcline but rather controls the speed of cycling around the hysteresis loop.

Another way to slow down the bursting is to add an ER to the model. Bursting with a physiological level of buffer ($f_{cyt} = 0.01$), but with an ER, is shown in Fig. 10C. Note that the level of buffer in the ER is also modest ($f_{er} = 0.01$, Table 2), but that c_{er} is nonetheless slow because the ER Ca^{2+} concentration is three orders of magnitude larger than that of the cytosol. The burst period, ≈ 35 sec, is much longer than that produced by the model with no ER (Fig. 10A). In addition, the cytosolic Ca^{2+} concentration no longer has a sawtooth shape (Fig. 10D), but instead has fast and slow components, in better agreement with experiment (Fig. 9).

Thus, while one often speaks casually of the ER acting to buffer Ca^{2+}, the model shows that the kinetic effect is quite different: Because buffering is rapid compared to the intrinsic timescale of c, it produces a uniform slowing of the c time course (compare Figs. 10B, 4B), whereas c_{er} is much slower than c and introduces a second slow kinetic component (Fig. 10D).

The new quantity in the model, c_{er}, has a sawtooth appearance, and is largely responsible for driving the bursting (Fig. 10D). This model prediction has not yet been tested experimentally, due to the technical difficulty of measuring the Ca^{2+} concentration in the ER, separate from the cytosolic Ca^{2+}, in an intact islet. Thus, a variable that we believe to be crucial to bursting in β-cells, the ER Ca^{2+}, is practically invisible to current experimental measurements, and can only be observed indirectly through its effects on the cytosolic Ca^{2+}.

The most robust feature in experiments is the biphasic decline of cytosolic Ca^{2+} during the silent phase (Fig. 9). The initial rapid decline reflects the abrupt cessation of Ca^{2+} entry, while the much slower decline that follows reflects release from the ER of Ca^{2+} that was taken up during the active phase. This interpretation is supported by the observation that the slow component disappears when SERCA pumps are blocked pharmacologically or genetically.

The addition of an ER compartment to the model also adds a great deal of flexibility to the system dynamics. That is, the period of bursting

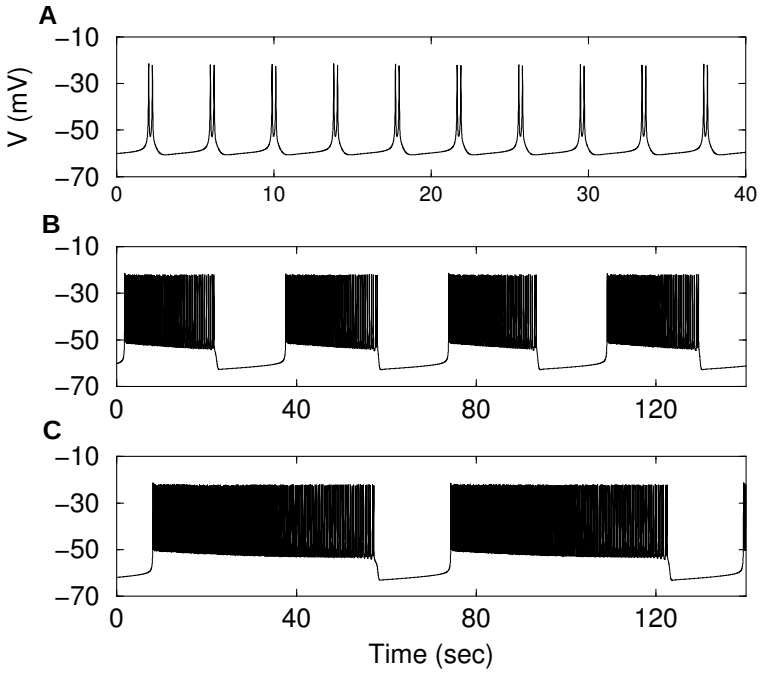

Fig. 11. The Chay-Keizer model with an ER can generate bursting with a wide range of periods. (**A**) Fast bursting is produced when $g_{K(Ca)} = 1000$ pS. (**B**) Slower bursting is produced when $g_{K(Ca)}$ is reduced to 500 pS. (**C**) Bursting becomes slower yet when $g_{K(Ca)}$ is reduced to 370 pS. The range of burst periods obtained by varying $g_{K(Ca)}$ is much smaller without an ER.

now ranges from a few seconds to more than a minute, and changes in period can be achieved by varying a single parameter, $g_{K(Ca)}$ (below we show that other parameters can also be varied to achieve a similar range of periods). From a biophysical perspective, if $g_{K(Ca)}$ is decreased it will take more Ca^{2+} to terminate the spiking since more K(Ca) channels must be activated, so the active phase duration will increase. Since the extra Ca^{2+} that accumulated during the active phase must be removed when the cell is hyperpolarized, the silent phase duration also increases. Thus, we expect the burst period to increase when $g_{K(Ca)}$ is reduced. While this would be true even without an ER, the role of the ER as a Ca^{2+} sink and source accentuates the effect of reducing $g_{K(Ca)}$, so that now the burst period can vary over orders of magnitude when $g_{K(Ca)}$ is varied modestly.

This is illustrated in Fig. 11. With $g_{K(Ca)} = 1000$ pS the bursting is fast, with a period of ≈ 3 sec (Fig. 11A). With $g_{K(Ca)} = 500$ pS the bursting is much slower and more islet-like, with period of ≈ 35 sec (Fig. 11B). Finally, with $g_{K(Ca)} = 370$ pS the bursting is slower still, now with period of ≈ 65 sec (Fig. 11C). Reducing $g_{K(Ca)}$ any further leads to continuous spiking. In contrast to Chay-Keizer with an ER, the burst period of Chay-Keizer without an ER (and with $f_{cyt} = 0.01$) is never more than a few seconds, regardless of the value of $g_{K(Ca)}$.

The dramatic effect of $g_{K(Ca)}$ can be be understood in terms of the fast/slow analysis. Figure 12A shows the z-curve and c-nullcline with $g_{K(Ca)} = 1000$ pS, the case in which fast bursting is produced. The second slow variable, c_{er}, is clamped at its average value, 181 μM. The relationship between z-curve and nullcline is essentially the same as for the Chay-Keizer model without an ER (Fig. 5). It is therefore not surprising that the bursting produced by this system is fast. Indeed, it is so fast that the oscillation amplitude in c_{er} is nearly zero, and one can clamp c_{er} at its average value without affecting the bursting.

The situation is quite different in Fig. 12B, where $g_{K(Ca)} = 500$ pS. The reduction in $g_{K(Ca)}$ has stretched the z-curve, moving the knees farther apart, and moving the homoclinic bifurcation farther to the right. (This can also be seen from Eqs. 11, 12.) As a result, the c-nullcline now intersects both the bottom branch and the periodic branch. Thus, during the silent phase the trajectory moves along the bottom branch until it reaches the intersection with the nullcline. At this point the trajectory stalls, and in the absence of an ER would remain at this point. However, c_{er} influences the c-nullcline: when c_{er} declines (as it would during the silent phase) the nullcline moves leftward. This can be seen by setting the right-hand-side of Eq. 13 to 0, viewing c_{er} as a parameter, to get

$$c = \frac{-\alpha I_{Ca} + p_{leak} c_{er}}{k_{pmca} + k_{serca} + p_{leak}} \tag{17}$$

on the c-nullcline. Eventually, the nullcline moves past the lower knee of the z-curve, and the trajectory escapes the silent phase and enters the active phase. Once again, though, the trajectory stalls, this time on the periodic branch during the active phase. However, as the cell spikes, Ca^{2+} accumulates in the ER, shifting the c-nullcline to the right. Eventually, the nullcline moves past the homoclinic bifurcation and the trajectory escapes the periodic branch to re-enter the silent phase.

Unlike the "classical" bursting of the Chay-Keizer model, where the

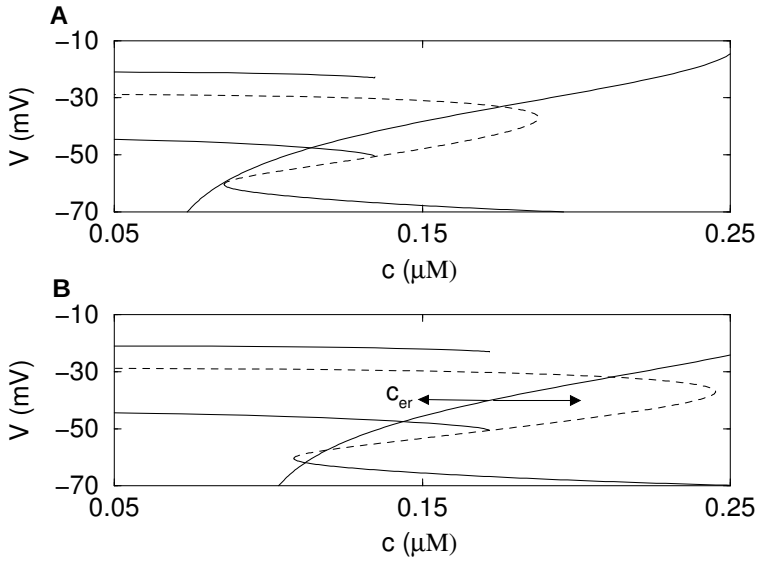

Fig. 12. The z-curve and c-nullcline for two different values of $g_{K(Ca)}$ and with c_{er} clamped. (**A**) With $g_{K(Ca)} = 1000$ pS the dynamics are similar to those of the Chay-Keizer model without an ER. Here, $c_{er} = 181$ μM. (**B**) Decreasing $g_{K(Ca)}$ to 500 pS stretches the z-curve, so that the knees are farther apart and the homoclinic bifurcation is further to the right. Now the trajectory stalls at intersections with the nullcline, awaiting slow changes in c_{er} to shift the nullcline to the right or the left (the nullcline moves to the right when c_{er} increases). Unlike the case above, if c_{er} is clamped bursting will not occcur. To make this diagram, c_{er} is set at 267 μM.

period was set by the time scale of c, the period of the bursting produced by the model with an ER is determined by the time scales of both c and c_{er}. The c time scale determines the time required for the trajectory to move along the z-curve until it reaches an intersection with the c-nullcline. The c_{er} time scale determines the time required for the nullcline to move past the knee during the silent phase and past the homoclinic bifurcation during the active phase. Since c_{er} changes more slowly than c, the burst period is dominated by the c_{er} time scale. Another factor in setting the burst period is the distance that the nullcline must travel for the trajectory to escape the silent or active phase. This is determined by how much the z-curve has been stretched, and thus by the value of $g_{K(Ca)}$. It is for this reason that such a large range of burst periods is achieved by varying this parameter. This scenario, in which the bursting is driven by activity-dependent oscillations

in two or more slow variables with disparate time scale, is called "phantom bursting" (Bertram *et al.*, 2000; Bertram and Sherman, 2004a).

It is interesting to note that the mechanism of phantom bursting, a slow variable translating a nullcline while the other "nullcline" (the z-curve) remains fixed, is similar to the mechanism for Chay-Keizer bursting itself when viewed in the nV-phase plane (Figs. 2 and 3). That is, bursting is produced when slow changes in c translate the V-nullcline while the n-nullcline remains fixed. The duration of the silent phase of the burst is determined primarily by the length of time required to move the lower knee of the V-nullcline past n-nullcline, so that there is no intersection on the lower branch. The active phase duration is also determined by the time required for changes in c to move the V-nullcline, this time past a homoclinic bifurcation point. Thus, the dynamics of phantom bursting recapitulate those of classical bursting at a higher level.

This suggests that we go on to view c as a component of the fast subsystem and consider a stack of phase-planes for different values of c_{er}. That is, we construct the bifurcation diagram of the V-n-c subsystem with respect to c_{er}. The z-curve for V with respect to c_{er} is then the curve on which V, n, and c are at steady state. It can be computed analytically by inverting Eq. 17 to get c_{er} in terms of c, and using Eqs. 11, 12 to express c in terms of V. Although the algebra is the same as before, when we viewed Eq. 17 as the equation for the c-nullcline and c as a slow variable, the point of view has changed. We now view c as a fast variable in equilibrium with V. The results are shown in Fig. 13 for the default parameters (A) and for increased ER leak (B). The oscillations become faster (see insets) because the the z-curve is squashed when the ER is partially depleted, decreasing the amplitude of c_{er}. This is the case that was considered by Chay (1996, 1997), in an early unappreciated example of phantom bursting. The increase in frequency is physiologically relevant for β-cells, representing part of the effect of acetylcholine to increase burst frequency and insulin secretion. Eqs. 11, 12, 17 also predict an increase in frequency when stores are depleted by reducing k_{serca}, another phenomenon seen in β-cells. See Bertram and Sherman (1994a) for details.

Varying k_{serca} and p_{leak} in proportion changes the rate of ER Ca^{2+} turnover without depleting or overfilling the ER. This also affects burst kinetics, with reduced turnover increasing burst frequency and also attenuating the slow tail in cytosolic Ca^{2+} (not shown). Thus, the ratio of ER flux to plasma membrane flux is an important parameter for adjusting β-cell models to produce realistic Ca^{2+} timecourses.

It may seem paradoxical that c_{er} is now the slow, negative-feedback variable because it does not affect the plasma membrane ion channels directly. The resolution of the paradox is contained in Eq. 17, which can be rewritten in the following form:

$$\begin{aligned} c &= \frac{-\alpha I_{Ca}(V)}{k_{pmca} + k_{serca} + p_{leak}} + \frac{p_{leak} c_{er}}{k_{pmca} + k_{serca} + p_{leak}} \\ &= c_{fast} + c_{slow} \end{aligned}$$

Thus, c can be decomposed into a fast component, which is in equilibrium with V and a slow component, which is in equilibrium with c_{er}. The slow rise and fall of c_{er} is communicated to $g_{K(Ca)}$ through the latter component. From this point of view, the increase in burst frequency as p_{leak} is increased reflects the increased efficiency with which the ER can influence $g_{K(Ca)}$. This "subtle inhibitory effect" of the ER was noted by Shorten and Wall (2000) in a model for pituitary corticotrophs exhibiting a range of non-square-wave bursting patterns. We point out that the ER does not play solely an inhibitory role: during the early part of the active phase, it blunts the rise of c and hence the activation of $g_{K(Ca)}$. This stimulatory effect prolongs the active phase, setting the stage for the delayed inhibitory effect that ultimately terminates the active phase.

6. Further Modifications to the Model

The model presented here is in reasonable agreement with the data in Fig. 9A, in which cytosolic Ca^{2+} rises throughout the active phase, but not with Fig. 9B, in which cytosolic Ca^{2+} declines towards the end of the active phase. Here we point to several modifications to the model in the current literature where this issue is addressed in different but complementary ways.

One way is to incorporate a hidden Ca^{2+} compartment that communicates with $g_{K(Ca)}$ and rises throughout the active phase (Goforth *et al.*, 2002). Such a compartment was postulated in order to account for data showing that block of SERCA pumps eliminated $I_{K(Ca)}$.

A second way is to incorporate a slow negative feedback process that is triggered by a rise in c but outlasts the rise in c. The hypothesis of Keizer and Magnus (1989) that the rise in c inhibits mitochondrial ATP production and hence reopens K(ATP) channels fits this description, and complements the effects of c_{er} in phantom-type models by sliding the V-c z-curve horizontally. (See Eqs. 11, 12 and Bertram and Sherman, 2004a).

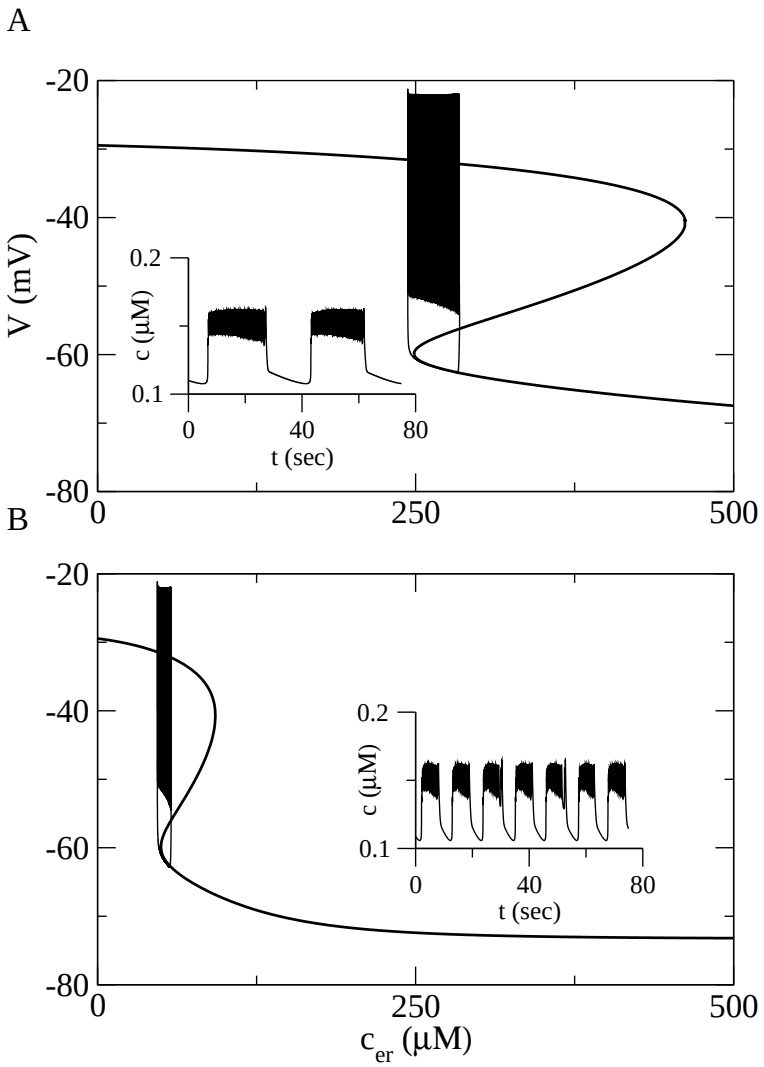

Fig. 13. Increasing ER efflux reduces c_{er} amplitude and increases burst frequency. BDs with respect to cer. A. $p_{leak} = 0.0002$, B. $p_{leak} = 0.001$ (insets, c vs. t.)

A third proposal is that c is not the primary ionic negative feedback process, but rather Na^+, which enters through the Na^+-Ca^{2+} exchanger and activates the Na^+-K^+ pump (Fridlyand *et al.* 2003).

Finally, data on compound oscillations ("bursts of bursts") in membrane

potential, cytosolic Ca^{2+}, and metabolic variables, such as oxygen, glucose, and mitochondrial membrane potential, have led to models in which glycolytic oscillations interact with electrical oscillations (Bertram et al, 2004c). These oscillations of metabolism would again slide the V-c z-curve, but, because they are independent of or only weakly dependent on cytosolic Ca^{2+}, the trajectory can be dragged outside the region of bistability. One consequence is that the oscillation may no longer be resettable by brief perturbations of membrane potential.

This is an area in which rapid development is in progress, but the dynamic foundation described here should continue to be useful in analyzing new models as they appear.

7. Discussion

We have traced the development of ideas on negative feedback by cytosolic Ca^{2+} via K(Ca) channels in β-cell models, starting with the Chay-Keizer model (1983). That model was successful in a number of ways, but its prediction of the kinetics of Ca^{2+} oscillations appeared to be fatally in disagreement with experiments showing both fast and slow components in c. Here we showed how adding a slow ER to Chay-Keizer could account for much of the discrepancy. The essential idea is that cytosolic Ca^{2+} is not very slow (viewed on the timescale of tens of seconds to minutes as found in β-cell electrical activity), but that the ER can impart an effective slow component.

More generally, one can speak of bi-directional communication between the plasma membrane and the ER. Oscillations of membrane potential cause oscillations of cytosolic Ca^{2+}, which are propagated into the ER. In turn, oscillations of ER Ca^{2+} modulate the kinetics of cytosolic Ca^{2+} and can thus affect membrane potential through cytosolic Ca^{2+}-dependent ion channels. This idea was used by Li *et al.* (1997) to explain how the ER promotes its own refilling after being emptied by agonists: when the ER is refilling, it takes up Ca^{2+} from the cytosol, deactivating K(Ca) channels and thus increasing action potential frequency and Ca^{2+} entry through the plasma membrane.

With regard to the β-cell, we caution that it has only been shown that K(Ca) channels can, with assistance from the ER, function as a slow negative feedback mechanism. While this hypothesis has also received some support from the identification for the first time of an appropriate non-voltage dependent K(Ca) channel in β-cells (Göpel *et al.*, 1999; Goforth

et al., 2002), it remains to be established experimentally that these K(Ca) channels play the role we have attributed to them.

We know that K(Ca) channels can not be solely responsible for bursting, because slow cytosolic Ca^{2+} oscillations persist in mice in which the low-affinity SERCA3 pump has been knocked-out (Arredouani *et al.* 2002). In this case, the cytosolic oscillations lack the slow tail seen normally (Fig. 9), which likely means that ER Ca^{2+} is flat. Thus, one can have oscillations of c without oscillations in c_{er}, raising the question of what role the latter serve. One intriguing possibility is that oscillations in the ER are more important for other functions of the cell, such as protein trafficking and gene expression, than for regulating cytosolic Ca^{2+} and membrane potential. This would be parallel to cytosolic Ca^{2+}, which serves both signaling and rhythmogenic roles.

Even if ER Ca^{2+} uptake is intact, the ER may fail to oscillate if it is too slow (eg. if σ_{er} is very small in Eq. 15). In the model decribed here, the ER only has an effect when it is sourcing or sinking Ca^{2+}. However, it is believed that β-cells, like many other cells, also possess store-operated channels (SOC) that carry an inward current directly activated by the level of c_{er}. SOC was previously proposed by us to mediate the response to acetylcholine-dependent store dumping (See Sherman, 1997) in a model with a very slow ER. Alternatively, when the ER is fast enough to oscillate in response to bursting, SOC can provide a gross depolarization that complements the increased frequency we showed here when ER efflux is activated (Fig. 13; Bertram and Sherman, 1994a). It has also been suggested that SOC itself can drive bursting, since influx would be attenuated by ER filling during the active phase and would recover during the silent phase (Chay, 1997 ; Fridlyand *et al.*, 2003). A different proposal is that Ca^{2+} influx triggers Ca^{2+} release from the ER by calcium-induced calcium release (CICR) and thus activates SOC to help sustain the active phase. This scenario seems unlikely, however, because disabling SERCA pumps increases, rather than decreases, the amplitude of c (Bertram and Sherman, 2004b.

The dynamical issues of having two negative feedback variables (here, cytosolic and ER Ca^{2+}) in a square-wave bursting model obviously generalize well beyond the β-cell. We have illustrated the concept of phantom bursting by means of bifurcation diagrams in the V-c plane, with c_{er} used as a parameter, and in the V-c_{er} plane, with c treated as a fast variable. The reader may wish to consider yet another point of view, the two-slow-variable plane (here, c vs. c_{er}), as described by Smolen *et al.* (1993).

References

1. A. Arredouani, Y. Guiot, J. C. Jonas, L. H. Liu, M. Nenquin, J. A. Pertusa, J. Rahier, J. F. Rolland, G. E. Shull, M. Stevens, F. Wuytack, J. C. Henquin, and P. Gilon. SERCA3 ablation does not impair insulin secretion but suggests distinct roles of different sarcoendoplasmic reticulum Ca^{2+} pumps for Ca^{2+} homeostasis in pancreatic β-cells. *Diabetes*, 51:3245–3253, 2002.
2. F. M. Ashcroft, D. E. Harrison, and S. J. H. Ashcroft. Glucose induces closure of single potassium channels in isolated rat pancreatic β-cells. *Nature*, 312:446–448, 1984.
3. F. M. Ashcroft and P. Rorsman. Type 2 diabetes mellitus: not quite exciting enough? *Human Mol. Gen.*, 13:R21–R31, 2004.
4. I. Atwater, C. M. Dawson, A. Scott, G. Eddlestone, and E. Rojas. The nature of the oscillatory behavior in electrical activity for pancreatic β-cell. In Georg Thieme, editor, *Biochemistry and Biophysics of the Pancreatic β-cell*, pages 100–107. Verlag, New York, 1980.
5. Paul M. Beigelman, Bernard Ribalet, and Illani Atwater. Electrical activity of mouse pancreatic beta–cells: II. Effects of glucose and arginine. *J. Physiol. (Paris)*, 73:201–217, 1977.
6. R. Bertram, M. J. Butte, T. Kiemel, and A. Sherman. Topological and phenomenological classification of bursting oscillations. *Bull. Math. Biol.*, 57:413–439, 1995.
7. R. Bertram, J. Previte, A. Sherman, T. A. Kinard, and L. S. Satin. The phantom burster model for pancreatic β-cells. *Biophys. J.*, 79:2880–2892, 2000.
8. R. Bertram, L. Satin, M. Zhang, P. Smolen, and A. Sherman. Calcium and glycolysis mediate multiple bursting modes in pancreatic islets. *Biophys. J.*, 87:3074–3087, 2004c.
9. R. Bertram and A. Sherman. A calcium-based phantom bursting model for pancreatic islets. *Bull. Math. Biol.*, 66:1313–1344, 2004a.
10. R. Bertram and A. Sherman. Filtering of calcium transients by the endoplasmic reticulum in pancreatic β-cells. *Biophys. J.*, 87:3775–3785, 2004b.
11. R. J. Butera Jr., J. Rinzel, and J. C. Smith. Models of respiratory rhythm generation in the pre-Bötzinger complex. I. Bursting pacemaker neurons. *J. Neurophysiol.*, 81:382–397, 1999.
12. T. R. Chay. Electrical bursting and luminal calcium oscillation in excitable cell models. *Biol. Cybern.*, 75:419–431, 1996.
13. T. R. Chay. Effects of extracellular calcium on electrical bursting and intracellular and luminal calcium oscillations in insulin secreting pancreatic β-cells. *Biophys. J.*, 73:1673–1688, 1997.
14. T. R. Chay and D. L. Cook. Endogenous bursting patterns in excitable cells. *Math. Biosci.*, 90:139–153, 1988.
15. T. R. Chay and J. Keizer. Minimal model for membrane oscillations in the pancreatic β-cell. *Biophys. J.*, 42:181–190, 1983.
16. Daniel L. Cook, Wayne E. Crill, and Daniel Porte, Jr. Plateau potentials in pancreatic islet cells are voltage-dependent action potentials. *Nature*,

286:404–406, 1980.
17. Richard FitzHugh. Impulses and physiological states in theoretical models of nerve membrane. *Biophys. J.*, 1:445–466, 1961.
18. L. E. Fridlyand, N. Tamarina, and L. H. Philipson. Modeling of Ca^{2+} flux in pancreatic β-cells: role of the plasma membrane and intracellular stores. *Am. J. Physiol. (Endocrinol. Metab.)*, 285:E138–E154, 2003.
19. P. B. Goforth, R. Bertram, F. A. Khan, M. Zhang, A. Sherman, and L. S. Satin. Calcium-activated K^+ channels of mouse pancreatic β-cells are controlled by both store and cytoplasmic Ca^{2+}: Experimental and theoretical studies. *J. Gen. Physiol.*, 120:307–322, 2002.
20. S. O. Göpel, T. Kanno, S. Barg, L. Eliasson, J. Galvanovskis, E. Renström, and P. Rorsman. Activation of ca^{2+}-dependent k^+ channels contributes to rhythmic firing of action potentials in mouse pancreatic β cells. *J. Gen. Physiol.*, 114:759–769, 1999.
21. Bertil Hille. *Ionic channels of excitable membranes*. Sinauer Associates, Sunderland, MA, 2001.
22. J. L. Hindmarsh and R. M. Rose. A model of neuronal bursting using three coupled first order differential equations. *Proc. R. Soc. Lond. B*, 221:87–102, 1984.
23. A. L. Hodgkin and A. F. Huxley. A quantitative description of membrane current and its application to conduction and excitation in nerve. *J. Physiol. (Lond.)*, 117:500–544, 1952.
24. E. M. Izhikevich. Neural excitability, spiking, and bursting. *Int. J. Bifur. Chaos*, 10:1171–1266, 2000.
25. Joel Keizer and G. Magnus. ATP-sensitive potassium channel and bursting in the pancreatic β cell. *Biophys. J.*, 56:229–242, 1989.
26. Joel Keizer and P. Smolen. Bursting electrical activity in pancreatic β cells caused by Ca^{2+}- and voltage-inactivated Ca^{2+} channels. *Proc. Natl. Acad. Sci. USA*, 88:3897–3901, 1991.
27. Y.-X. Li, S. S. Stojilkovic, J. Keizer, and J. Rinzel. Sensing and refilling calcium stores in an excitable cell. *Biophys. J.*, 72:1080–1091, 1997.
28. E. K. Matthews and M. D. L. O'Connor. Dynamics oscillations in the membrane potential of pancreaticislet cells. *J. Exp. Biol.*, 81:75–91, 1979.
29. C. Morris and H. Lecar. Voltage oscillations in the barnacle giant muscle fiber. *Biophys. J.*, 35:193–213, 1981.
30. J. Nagumo, S. Arimoto, and S. Yoshizawa. An active pulse transmission line simulating nerve axon. *Proc. IRE.*, 50:2061–2070, 1964.
31. R. E. Plant. The effects of Ca^{2+} on bursting neurons. *Biophys. J.*, 21:217–237, 1978.
32. J. Rinzel. A formal classification of bursting mechanisms in excitable systems. In E. Teramoto and M. Yamaguti, editors, *Mathematical Topics in Population Biology, Morphogenesis and Neurosciences*, volume 71 of *Lecture Notes in Biomathematics*, pages 267–281, Berlin, 1987. Springer–Verlag.
33. J. Rinzel, T. R. Chay, D. Himmel, and I. Atwater. Prediction of the glucose-induced changes in membrane ionic permeability and cytosolic Ca^{2+} by mathematical modeling. In I. Atwater, E. Rojas, and B. Soria, editors, *Bio-*

physics of the Pancreatic β-Cell, pages 247–263. Plenum Publishing Co., New York and London, 1986.

34. J. Rinzel and Y. S. Lee. On different mechanisms for membrane potential bursting. In H. G. Othmer, editor, *Nonlinear oscillations in biology and chemistry*, volume 66 of *Lecture Notes in Biomathematics*, pages 19–33, Berlin, 1985. Springer–Verlag.
35. A. Sherman. Calcium and membrane potential oscillations in pancreatic β-cells. In H. G. Othmer, F. R. Adler, M. A. Lewis, and J. C. Dallon, editors, *Case Studies in Mathematical Modeling—Ecology, Physiology, and Cell Biology*, pages 199–217. Prentice-Hall, New Jersey, 1997.
36. P. R. Shorten and D. J. N. Wall. A Hodgkin-Huxley model exhibiting bursting oscillations. *Bull. Math. Biol.*, 62:695–715, 2000.
37. P. Smolen and J. Keizer. Slow voltage inactivation of Ca^{2+} currents and bursting mechanisms for the mouse pancreatic β–cell. *J. Membrane Biol.*, 127:9–19, 1992.
38. P. Smolen and A. Sherman. Phase independent resetting in relaxation and bursting oscillators. *J. theor. Biol.*, 169:339–348, 1994.
39. P. Smolen, D. Terman, and J. Rinzel. Properties of a bursting model with two slow inhibitory variables. *SIAM J. Appl. Math.*, 53:861–892, 1993.
40. J. Tabak, J. Rinzel, and M. J. O'Donovan. The role of activity-dependent network depression in the expression and self-regulation of spontaneous activity in the developing spinal cord. *J. Neurosci.*, 21:8966–8978, 2001.
41. David Terman. The transition from bursting to continuous spiking in excitable membrane models. *J. Nonlinear Sci.*, 2:135–182, 1992.
42. M. Valdeolmillos, R. M. Santos, D. Contreras, B. Soria, and L. M. Rosario. Glucose-induced oscillations of intracellular Ca^{2+} concentration resembling bursting electrical activity in single mouse islets of Langerhans. *FEBS Lett.*, 259:19–23, 1989.
43. B. van der Pol and J. van der Mark. The heartbeat considered as a relaxation oscillation, and an electrical model of the heart. *Phil. Mag.*, 6:763–775, 1928.
44. M. Zhang, P. Goforth, R. Bertram, A. Sherman, and L. Satin. The Ca^{2+} dynamics of isolated mouse β-cells and islets: Implications for mathematical models. *Biophys. J.*, 84:2852–2870, 2003.